Microwave-induced crystallization of AC/TiO2 for improving the performance of rhodamine B dye degradation

Microwave-induced crystallization of AC/TiO_2 for improving the performance of Rhodamine B dye degradation

Fei Tian[a], Zhansheng Wu[a,*], Qiuyu Chen[a], Yujun Yan[a], Giancarlo Cravotto[b], Zhilin Wu[b]

aSchool of Chemistry and Chemical Engineering, Shihezi University, Shihezi 832003, PR China

bDipartimento di Scienza e Tecnologia del Farmaco, University of Turin, Torino 10125, Italy

Titanium dioxide (TiO_2) deposition on activated carbon (AC) is widely used for pollutant photodegradation. In this study, a simple and efficient method for preparing AC/TiO_2 composites under microwave irradiation was developed for photocatalytic degradation of Rhodamine B (RhB) under UV light. Results of X-ray diffraction, scanning electron microscopy, and transmission electron microscopy revealed that TiO_2 nanoparticles are anatase and rutile, with a spherical shape and a particle size of 20–50 nm and are well distributed on the AC surface. The UV-vis spectrum of TiO_2 coated on AC showed an evident red-shift and exhibited stronger optical absorption capacity than pure TiO_2. The AC/TiO_2 nanoparticles prepared at a microwave power of 700 W for 15 min exhibited 98% efficiency in removing RhB dye under UV irradiation for 30 min. The high photocatalytic activity of AC/TiO_2-700 W could be mainly attributed to the high sorption capacity of the mesoporous carbon material and high TiO_2 content, which could produce higher quantity of ·OH. This study provides a rapid synthesis technique to prepare AC/TiO_2 and a novel method to improve photocatalytic efficiency via synergistic effect for other catalytic systems.

Keywords: anatase-rutile; microwave irradiation; mesoporous carbon; photocatalysis; adsorption.

1. Introduction

Water pollution has become one of the most serious problems of our society. Organic poisonous contaminants including xanthene dyes are of the most harmful water pollutants.

Rhodamine B (RhB) is an important xanthene dye used as a laser and colorant for textile materials because of its good stability [1]. According to the International Agency for Research on Cancer, RhB may cause acute and chronic poisoning through ingestion, inhalation, and skin contact. This poisonous organic contaminant can be removed from water through various methods, such as chemical precipitation, advanced oxidation, electrochemical techniques, and ion exchange [2-5]. As applications of these methods are limited because of technical difficulties or environment hazards [6-7], an effective and optimal strategy to rapidly remove RhB from water and wastewater must be developed.

Semiconductor photocatalysts are the most cost-optimal, effective, and environment friendly material for applications directed toward energy and environmental concerns [8-10]. Among these photocatalysts, titanium dioxide (TiO_2) is widely used in heterogeneous photocatalysis to degrade organic pollutants in water and air because it features nontoxicity, chemical and biological inertness, and low cost [11-16]. TiO_2 nanoparticles are generally synthesized through different methods, such as hydrothermal, sol–gel, and electrochemical [17-18]. These methods involve a conventional thermal treatment process using a high-temperature furnace for annealing [19-22]. Nevertheless, heating a furnace consumes a high amount of energy and time. In this regard, microwave–hydrothermal technique, as a novel and fast method, has attracted much interest in recent years [23]. Microwaves exhibit potential for various applications and the use of microwaves provides a fast heating process, thereby saving energy and money and shortening synthesis time [24, 25]. Chen et al. [26] reported that the reaction time for TiO_2 crystallization decreased from 16 h via the hydrothermal process to 80 min via microwave irradiation.

In most of the cases, the degradation efficiency of TiO_2 is relatively low in practical

application because of its small surface area and the poor adsorption of organic poisonous contaminants onto it [27, 28]. TiO_2 supported on activated carbon that provided the crystalline framework to support TiO_2 nanoparticles, has been adopted in removal of organic contaminants. Pastravanu et al. [29] synthesized TiO_2-coated carbon samples that exhibited high photocatalytic activity, such that 92% of methyl orange (MO) was degraded after 170 min of UV irradiation. The studies showed that the microwave-assisted synthesis requires a shorter reaction time than conventional methods. Nevertheless, to the best of our knowledge, limited studies have used microwave radiation to synthesize AC/TiO_2 for rapid photocatalysis of RhB. Furthermore, no studies have reported the effects of microwave conditions on the properties of TiO_2 loaded on AC and on the catalytic performance of AC/TiO_2.

In this study, AC/TiO_2 was synthesized via a simple, fast, and efficient one-step method under different microwave conditions. Brunauer–Emmett–Teller (BET) surface area, X-ray diffraction (XRD), scanning electron microscopy (SEM), transmission electron microscopy (TEM), X-ray photoelectron spectroscopy (XPS), Fourier-transform infrared (FTIR) spectroscopy, and UV-vis diffusion reflection spectroscopy (DRS) were utilized to assess the photocatalytic performance of the enhanced catalyst. In addition, photocatalytic degradation of RhB by AC/TiO_2 and bare TiO_2 was evaluated under different microwave powers.

2. Materials and methods

2.1 Preparation of AC/TiO_2

AC was prepared based on our precious study [30]. It was using a microwave oven (MM823LA6-NS, Midea) at a frequency of 2.45 GHz. A mixture of solid KOH (10 g) and dried coal at a ratio of 1:1 was placed in a quartzose tube in a microwave reactor and activated under

vacuum atmosphere at 693 W for 10 min. The KOH is intercalated to the carbon matrix responsible for both stabilization and widening of the spaces between the carbon atomic layers. Metallic potassium formed during redox reaction can be intercalated into the carbon walls independently of the structural order responsible for separation and degradation of graphitic layers thus develop the microporosity and mesoporosity. The obtained AC samples were pretreated by adding into HNO_3 solution with 24 h. The mixture was filtered using distilled water until they became neutral. The pretreated AC was then dried and stored until use.

The TiO_2 gel/sol was obtained by conventional sol-gel method. All reagents were of analytical grade and used without further purification. In typical synthesis process, 30 mL of tetrabutyl orthotitanate (TBOT) was dissolved in anhydrous alcohol (EtOH) in proportion of 1:1 (volume ratio). This solution was thoroughly stirred for 40 min and named solution A. Solution B was prepared by mixing 14 mL of glacial acetic acid and 7 mL of distilled water in 35 mL of absolute alcohol. Solution B was added to solution A dropwise and continuously stirred for 1 h. Then it was obtained pale yellow clear TiO_2 sol.

AC/TiO_2 nanoparticles were prepared as follows. Pretreated AC (10 g) was added into TiO_2 sol (100 g) [31]. The mixture was placed in an oven at 100 °C for 24 h. After solidification, AC/TiO_2 was prepared under different microwave conditions: irradiation at 100 W for 30 min or at 300–900 W for 15 min based on results of preliminary experiment, the microwave oven followed a working cycle of 6 s on and 24 s off (20% power). The resulted samples were noted as AC/TiO_2-100 W, AC/TiO_2-300 W, AC/TiO_2-500 W, AC/TiO_2-700 W and AC/TiO_2-900 W.

2.2 Catalyst characterization

The prepared samples were characterized through XRD on a Rigaku D/Max-2500/PC powder

diffractometer. Each sample powder was scanned using Cu-$K\alpha$ radiation with an operating voltage of 40 kV and an operating current of 200 mA. The scan rate of 5°/min was applied to record the patterns in the range of 10-80° at a step of 0.02°. XPS analysis of samples was conducted using a PHI5700 ESCA system equipped with a Mg $K\alpha$ X-ray source (1253.6 eV) under a vacuum pressure $<10^{-6}$ Pa. Pass energy was set as 187.85 and 29.35 eV for the survey and high-resolution spectra, respectively. The XPS spectra of the samples were calibrated by taking the graphitic carbon peak as 284.6 eV. The surface micromorphologies of AC and AC/TiO_2 were characterized through SEM (S4800, Hitachi LTD) at an accelerating voltage of 15 kV. TEM was performed on a Tecnai G2 F20 microscope at 100 kV. FTIR spectra were recorded with a Bruker Vertex FTIR spectrometer, resolution of 2 cm^{-1}, in the range of 4000-400 cm^{-1} by KBr pellet technique. The UV-vis DRS were obtained with a powder UV-vis spectrophotometer (U-4100, Hitachi LTD). Specific surface area (SBET, $m^2 \cdot g^{-1}$) was calculated using the BET equation, and total pore volume (V_t, $m^3 \cdot g^{-1}$) was evaluated by converting the adsorption amount at $P/P_0 = 0.95$ to the volume of liquid adsorbate. Micropore volume, micropore surface area, and external surface area were determined using t-plot method. Average pore size (r, Å) was estimated with the following equation:

$$r = \frac{4V_t}{SBET} \quad (2\text{-}1)$$

The formation rate of ·OH at photo-illuminated sample/water interface was detected by the Photoluminescence (PL) technique using terephthalic acid (TA) as a probe molecule. PL spectroscopy of synthesized products was taken at room temperature on a Hitachi F2500 spectrofluorometer using a Xe lamp with an excitation wavelength of 325 nm.

2.3 Photocatalytic activity for RhB degradation

Photocatalytic experiments were performed to investigate UV-assisted degradation of RhB solution by AC/TiO_2 at room temperature by using a 1000 W UV lamp with 365 nm wavelength. In a typical test, 0.01 g of catalyst was added to 50 mL of RhB solution (30 mg/L, pH=6.8). The mixture was kept in the dark for 30 min to allow adsorption of RhB on the AC/TiO_2 surface. The mixture was then irradiated under UV lamp to degrade RhB. The distance between the reactor and lamp housing is 8.5 cm.

The removal rate (η) of RhB can be calculated as follows:

$$\eta = \frac{C_o - C_t}{C_o} \times 100 \quad (2\text{-}2)$$

where C_o and C_t are the concentrations of RhB at initial and different irradiation times, respectively.

3. Results and discussion

3.1 XRD spectra

Fig. 1 depicts the XRD patterns of neat AC as support and AC/TiO_2. No diffraction patterns from carbon species were detected in all samples. All AC/TiO_2 composites exhibited peaks at 2θ = 25.281°, which is a characteristic of the anatase phase (101). The average crystallite sizes of the anatase and rutile phase calculated from the Scherrer equation are listed in Table 1. The calculated crystal sizes of the samples range from 10 nm to 50 nm. These results indicated that TiO_2 loaded on the AC powder are nanoparticles.

Fig. 1 shows that after 100 W of microwave radiation, the XRD peaks of the TiO_2 anatase phase could be detected in the powder sample without other phase. When the microwave power was increased, the mixed crystals of anatase [JCDPS No. 21-1272] and rutile [JCDPS No. 21-1276] [11] were observed (Fig. 1 (b)-(e)). The anatase to rutile phase transformation is generally

considered as nucleation growth process during which the rutile nuclei are formed within the anatase phase [4]. Thus, various crystallite size of anatase can be obtained in the formation process of rutile under different prepared condition. With an increase of the microwave power from 300 W to 900 W, the content of rutile increased see in Table 1. As the energy position of the anatase conduction band edge is higher than that of rutile, the photogenerated electrons migrate from anatase to rutile and the positive holes migrate from rutile to anatase. Hence, low electron–hole recombination can enhance the photocatalytic activity of the mixed-phase TiO_2. When the microwave power was increased, the degree of crystallinity in the structural order also increased (narrower peaks) [8], while no further improvement was observed at power exceeding 700 W. As photoreactivity requires a balance among crystallinity, specific surface area, and porosity, we prepared amorphous TiO_2 gel through fast microwave crystallization and improved the crystallinity of TiO_2 spheres with minimal loss in the SBET and porosity. Compared with as-synthesized TiO_2 (for 700 W with 15 min), AC/TiO_2-700 W show the same peaks. Thus, combination with AC does not influence the crystal structure of the host TiO_2 material. The XRD results demonstrated that microwave is a promising synthesis technique to enhance the crystallinity of AC/TiO_2.

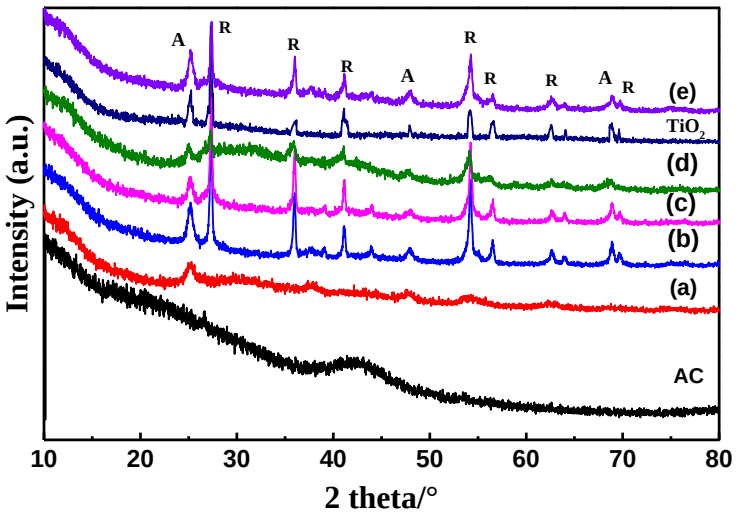

Fig. 1 XRD patterns of AC, TiO_2 (for 700 W with 15 min) and AC/TiO_2: (a) AC/TiO_2-100 W, (b)

AC/TiO_2-300 W, (c) AC/TiO_2-500 W, (d) AC/TiO_2-700 W, (e) AC/TiO_2-900 W. A: anatase crystalline phase of TiO_2 and R: rutile crystalline phase of TiO_2.

3.2 BET

Surface areas and pore size distribution of the samples were determined through N_2 sorption measurements. SBET, V_t, and mean pore diameter (d_{mean}) obtained from N_2 adsorption/desorption measurements are presented in Table 1. Pure AC presented large SBET and V_t, whereas AC/TiO_2 demonstrated decreased SBET of more than 50% and decreased V_t. This phenomenon could be due to the generated TiO_2 crystals and other solid matter that covered the AC surface and blocked the pore structure. The BET surface of AC/TiO_2 evidently increased when the microwave power increased from 100 to 700 W. This phenomenon is probably due to sublimation of the covered solid matter which reduced the blocked surface of AC, thereby increasing the exposed surface area. When the microwave power was increased to 900 W, the SBET of AC/TiO_2 decreased because the reunion of titanium dioxide crystals and collapse of the AC structure induced by high temperatures.

Fig. 2 shows the N_2 adsorption–desorption isotherms of uncoated and TiO_2-coated AC and the pore size distribution (inset) calculated by BJH method. A unimodal distribution centralized at 3.8 nm was observed in AC and AC/TiO_2 (300–900 W) powders, whereas AC/TiO_2-100 W showed very small mesopores of approximately 3.414 nm. This characteristic could be due to incomplete crystal formation of TiO_2 sol at a low microwave power (100 W). Although AC and AC/TiO_2 showed similar peaks, the latter presented significantly lower intensity, indicating that the carbon pore entrance was blocked by TiO_2 nanoparticles. Data on average pore diameter indicated that all prepared photocatalysts are mesoporous materials. The mesoporosity of AC/TiO_2 was significantly reduced when the microwave power was increased to 900 W, which could be due to the destroyed AC pores.

According to IUPAC classification, the N_2 adsorption isotherms of the samples are essentially of type IV with a type-H_4 hysteresis loop (Fig. 2). This characteristic indicates that synthesized materials present mesoporous structure with slit-shaped pores, which is similar to the result obtained by Pastravanu et al. [29]. In the mesoporous carbon sample, AC/TiO_2 exhibited almost the same shape with a small difference in N_2 adsorbed volume. This characteristic is an indication of carbon mesopore filling with titania nanoparticles that resulted in reduced SBET (Table 1). However, during TiO_2 deposition, the hysteresis shape tended toward an H_2-type, suggesting the evolution of slit-shape into a complex pore structure. All isotherms showed a significant hysteresis at the relative pressure P/P_0 between 0.05 and 0.2, which indicates the existence of mesoporosity in the nanospheric samples [1].

Table 1 The characterization results of different samples

Samples	SBET[a] (m^2/g)	V_t[b] (cm^3/g)	d_{pore}[c] (nm)	D_{hkl}[d] (nm)	$d_{particle}$[e] (nm)	A/R[f]	M[g] (%)
AC	1915	1.020	3.829	/	/	/	/
AC/TiO_2-100W	332	0.196	3.414	11.6	12	A	30.81
AC/TiO_2-300W	364	0.215	3.828	22.6/24.5	30	34/66	42.97
AC/TiO_2-500W	498	0.237	3.825	46.8/49.3	45	39/61	52.56
AC/TiO_2-700W	547	0.362	3.828	17.9/22.9	17	47/53	58.72
AC/TiO_2-900W	190	0.121	3.829	48.3/50.2	45	78/22	47.51

a BET specific surface area.
b Total pore volume taken at $P/P_0 = 0.98$.
c Mean pore diameter calculated with BJH method.
d Crystallite size of anatase and rutile calculated with Scherrer equation.
e Mean particle size of TiO_2 determined from TEM.
f Phase ratio of anatase and rutile.
g Percentage composition of TiO_2 calculated by ash method

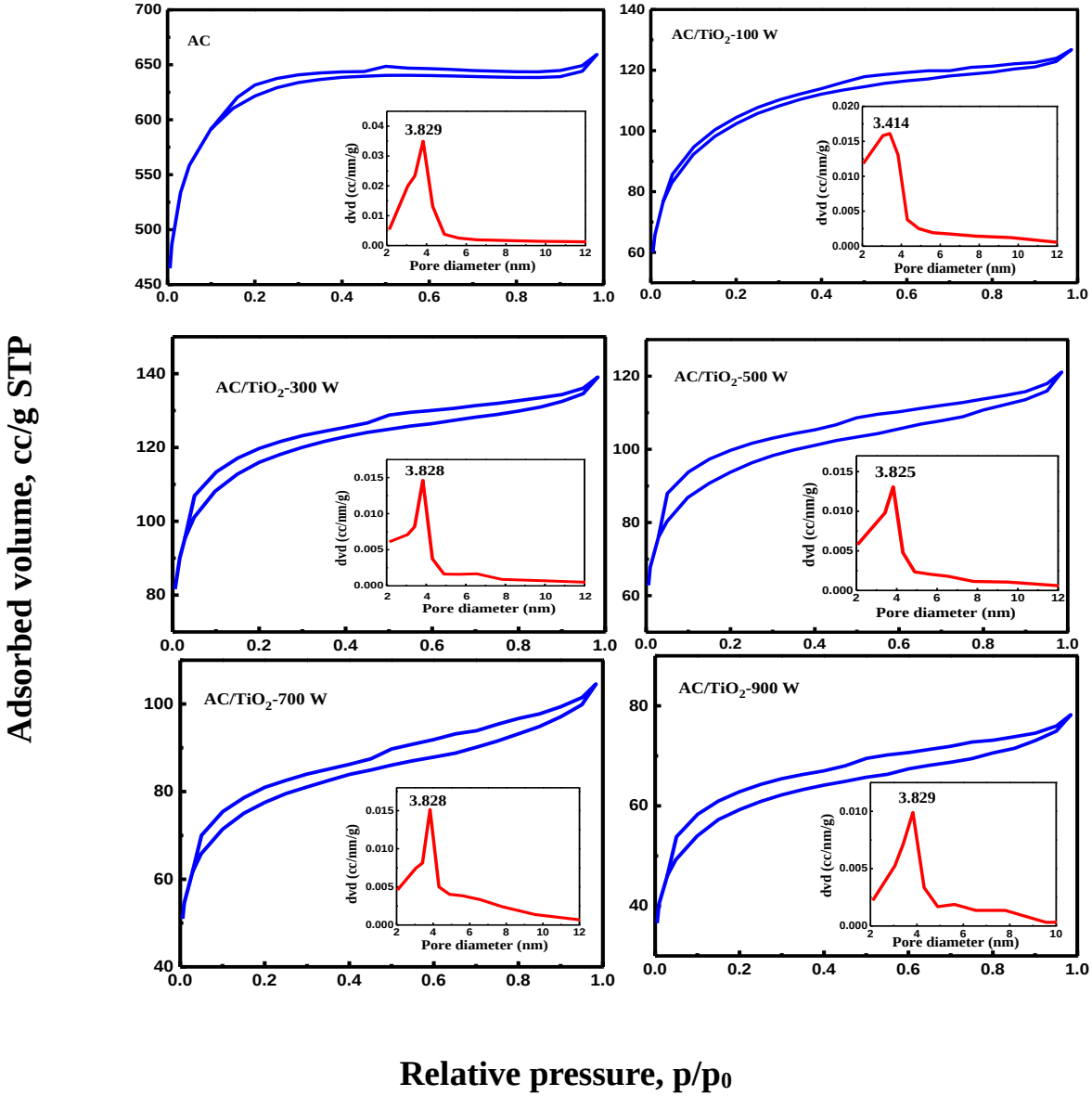

191

192 Fig. 2 Nitrogen adsorption-desorption BET isotherms and pore size distribution curves (inset) of AC and

193 AC/TiO_2.

194 **3.3 SEM**

195 The morphology of the synthesized samples was examined through SEM, and the typical

196 SEM micrographs of AC, TiO_2, and AC/TiO_2 are shown in Fig. 3. The uncoated AC particle

197 surface was smooth. By contrast, for AC/TiO_2, TiO_2 particles were distributed on the AC surface

198 and no significant changes in the internal morphology of AC were observed as shown in the SEM

micrographs (Fig. 3 (a)–(e)). Changing the microwave power resulted in different distributions and covered areas of TiO_2 on the AC surface, although a portion on the AC surface remained unoccupied as shown in the lower magnification micrograph on the left side of Fig. 3; this finding is consistent with BET results. The high-magnification images on the right side of Fig. 3 indicate that the synthesized TiO_2 features 20 to 50 nm size and a spherical shape. When the microwave power was increased from 100 to 700 W, more TiO_2 particles formed on the AC surface. Under microwave preparation conditions of 700 W for 15 min, photocatalytic particles were relatively uniform, spherical in shape, and better dispersed on AC. And compared with TiO_2, the coated-TiO_2 particles become pronounced and coarse by pitch treatment and the size of the particles is kept large. While the microwave power rising to 900 W, the TiO_2 particle was highly agglomerated due to the low stability of the small-sized particles, and leading to the TiO_2 gather on the surface of AC.

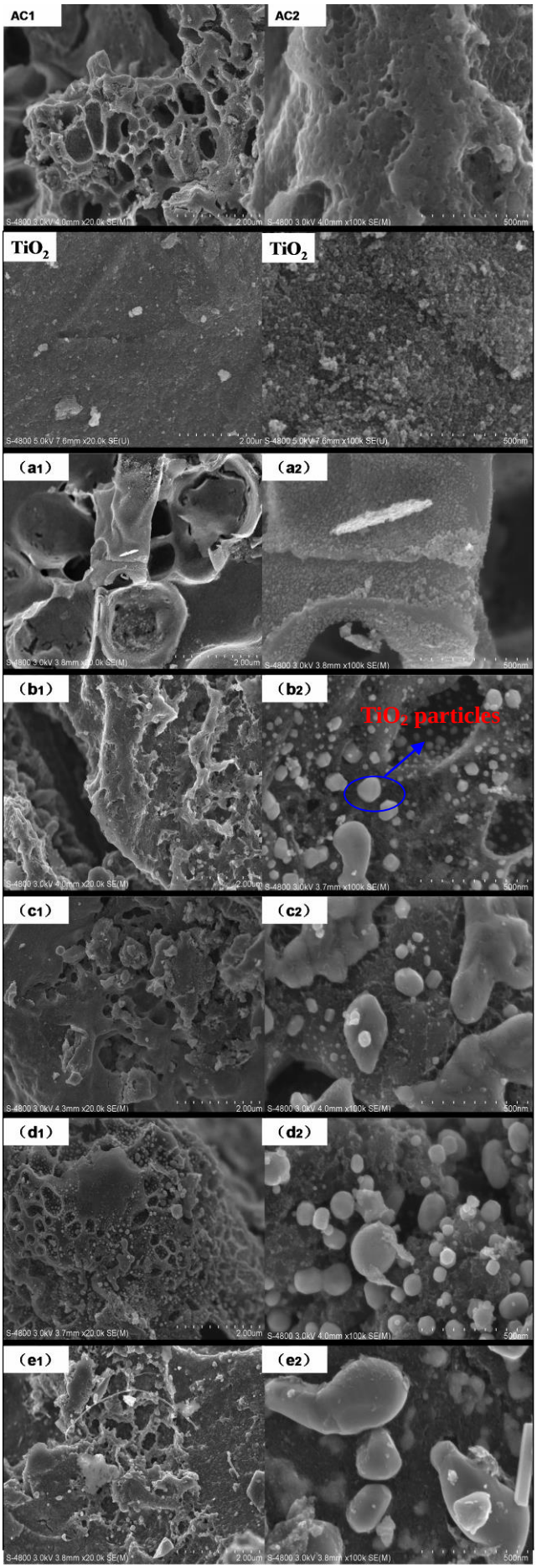

211

Fig. 3 SEM of AC, TiO_2 and AC/TiO_2: (a) AC/TiO_2-100 W, (b) AC/TiO_2-300 W, (c) AC/TiO_2-500 W, (d) AC/TiO_2-700 W, (e) AC/TiO_2-900 W.

3.4 TEM

Fig. 4 shows the TEM micrographs of AC/TiO_2 samples recorded under different magnifications. Under low magnification, the TEM micrograph showed spherical TiO_2 particles distributed on the AC surface, which was also observed in the SEM measurements. Under high magnification, the particle sizes (nm) of the spherical-shaped TiO_2 crystals are distributed as follows: (a) 10–15 nm, (b) 20–50 nm, (c) 40–50 nm, (d) 15–20 nm, and (e) 40–50 nm; these findings are consistent with the XRD results. Only a small amount of TiO_2 particles formed on the AC surface at a microwave power of 100 W for 30 min, and the particle size of TiO_2 is very small with an unstable morphology and structure. Thus, a very low microwave power is not conducive to the formation of the TiO_2 core-shell structure. The amount of TiO_2 particles loaded on AC increased when the microwave power increased from 100 to 700 W (Table 1). The images showed that TiO_2 nanoparticles are uniform in size and shape, free from aggregation, and well-dispersed on AC when the preparation power was 700 W. However, when the microwave power was increased to 900 W, TiO_2 spheres with close interconnection showed serious agglomeration. Thus, the AC/TiO_2-700 W photocatalyst could provide the free surface of AC for dye adsorption on the microspheres, and the transfer of the dye around TiO_2 resulted in enhanced dye degradation.

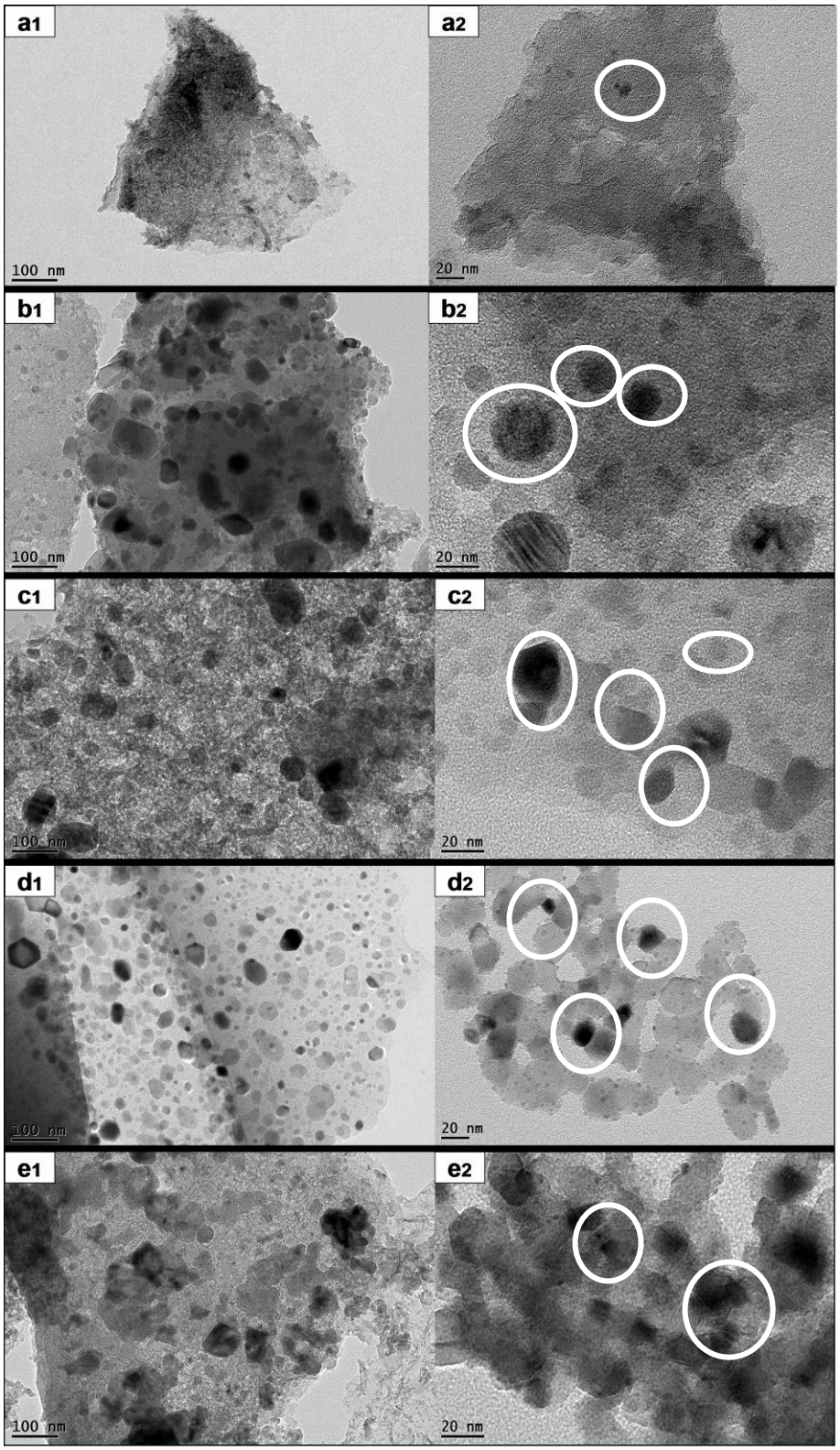

Fig. 4 TEM of AC/TiO_2: (a) AC/TiO_2-100 W, (b) AC/TiO_2-300 W, (c) AC/TiO_2-500 W, (d) AC/TiO_2-700 W, (e) AC/TiO_2-900 W.

3.5 FTIR

We performed FTIR experiments to determine the surface activity of the catalysts. Fig. 5

shows the FTIR spectra of AC and AC/TiO_2 nanocomposites in the spectral region from 450 to 4000 cm^{-1}. The strong peak of the AC/TiO_2 nanocomposites around 3425 and 2360 cm^{-1} are attributed to asymmetric stretching vibration of O–H, which are similar to those of the AC samples. This finding indicates that no dehydroxylation occurred during formation of AC/TiO_2 nanocomposites. The improved hydrophilicity and wettability of the mesoporous carbon are advantageous for organic adsorption from aqueous solutions [28]. The main reason for this benefit may be that the very short heating time and the activity of rapid resolidification of molten phases, in conjunction with the aqueous environment, avoids the dehydroxylation of AC. The comparison of the curves of AC and AC/TiO_2 and FTIR results suggest that the formation of titania nanoparticles in the AC/TiO_2 nanocomposites did not alter the structure or phase of the AC crystals. The broad absorption band in the range of 400–800 cm^{-1} characterizes the Ti–O and Ti–O–Ti vibration of anatase, which confirms the formation of TiO_2. Moreover, the appearance of bands at 1080 cm^{-1} indicates the clear formation of the Ti–O–C bonds, suggesting that TiO_2 binds to the mesoporous carbon surface [29].

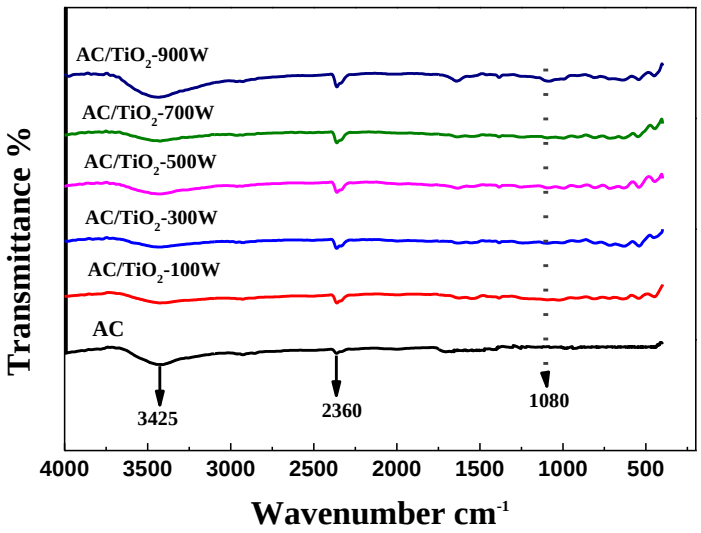

Fig. 5 FTIR spectra of AC and AC/TiO_2: (a) AC/TiO_2-100 W, (b) AC/TiO_2-300 W, (c) AC/TiO_2-500 W, (d) AC/TiO_2-700 W, (e) AC/TiO_2-900 W.

3.6 XPS

To understand the oxidation states of Ti, we conducted XPS measurements of TiO_2 (prepared for 700 W with 15 min) and AC/TiO_2-700 W (Fig. 6). Ti 2p 1/2 and Ti 2p 3/2 peaks were observed in pure TiO_2, with binding energies of 465.3 and 459.75 eV, respectively, and the binding energies of these peaks in the AC/TiO_2 samples shifted toward 465.2 and 459.5 eV, respectively. The observed range of the 2p binding energy values for TiO_2 and AC/TiO_2 samples indicates that Ti is in the +4 oxidation state [28]. Therefore, Ti in the AC/TiO_2 nanocomposites is the TiO_2 derived from titania. The XPS results confirmed the formation of titania in the AC/TiO_2 nanocomposites and indicated the stability of the TiO_2 nanocomposite under the reaction condition.

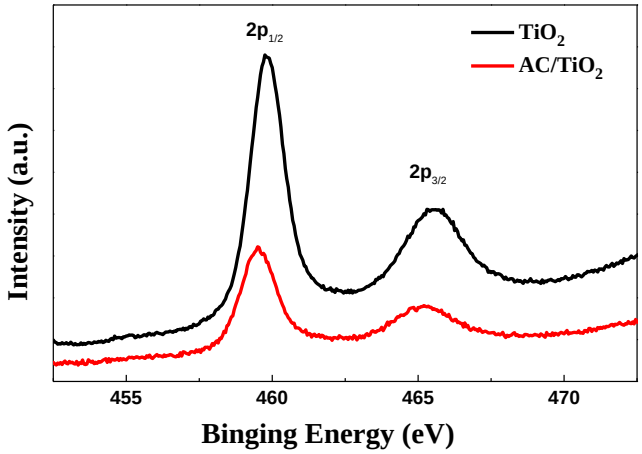

Fig. 6 XPS of Ti 2p in TiO_2 and AC/TiO_2-700 W.

3.7 UV-vis spectra

The UV-vis DRS of TiO_2 (prepared for 700 W with 15 min) and AC/TiO_2 samples are shown in the inset Fig. 7. With TiO_2 loaded on AC, the absorbance in the visible region was enhanced. Pure TiO_2 showed an intrinsic absorption with light wavelength shorter than 390 nm and almost no absorption in visible light with wavelength ranging from 400 to 800 nm. This adsorption is mainly attributed to the inter-band transition of TiO_2 [11]. The light absorption edge of

AC/TiO_2-700 W was 412 nm, with a remarkable red shift to the visible range compared with the spectrum of pure TiO_2. This change influenced the effective band gap of the photocatalyst. TiO_2 is known as an indirect semiconductor, for which the relation between absorption coefficient (a) and the incident photon energy (hv) can be written as $a=B_i (hv\text{-}Eg)^2/hv$ [3], where B_i is the absorption constant for indirect transitions. Plots of $(ahv)^{1/2}$ versus hv from the spectral data are presented of Fig. 7. Thus, the sample AC/TiO_2 was found to have band gap 2.67 eV which was lower than the band gap of the initial titania powder (2.91 eV) and for this reason it is expected the AC-TiO_2 to be photocatalytically active under visible light. Moreover, Zhang [15] reported that absorbance in the presence of AC/TiO_2 was higher than that in the presence of AC.

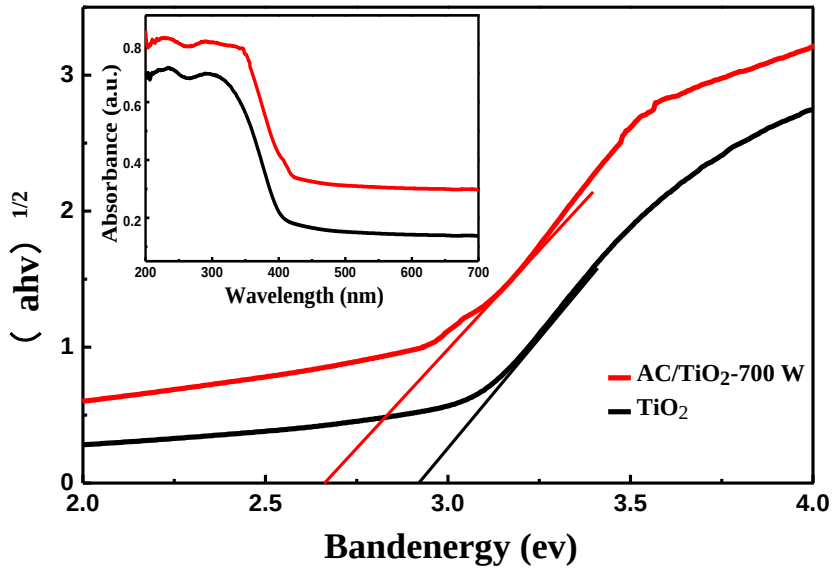

Fig. 7 Diffuse reflectance absorption spectra of TiO_2 and AC/TiO_2-700 W.

3.8 Photocatalytic activity

The activities of the synthesized nanocomposites were evaluated through photodegradation of RhB aqueous solution (30 mg/L) under UV irradiation at 365 nm (Fig. 8). A blank experiment without any photocatalyst (photolysis) was conducted for comparison. No evident photodegradation of RhB was observed after 30 min of irradiation in the absence of photocatalyst

285 (direct photolysis). The pure photolytic removal efficiency of the as-synthesized TiO_2 sample (for
286 700 W with 15 min) was 18.52%, and the adsorption efficiency of AC was 20%, exclusive of the
287 30 min dark reaction. The removal efficiency of AC/TiO_2 composite samples presented high
288 photolytic removal efficiency that ranged from 37 to 95% (Fig. 8 (inset)). TiO_2 loaded on AC
289 exhibited very high photocatalytic degradation efficiency compared with AC and pure TiO_2. The
290 substantially decrease in RhB concentration in the aqueous solution can occur in a
291 physical–chemical phenomenon, such as adsorption by AC and photocatalytic decomposition by
292 TiO_2. The activated carbon played a role of adsorption at the ratio 1:10 (AC and TiO_2-sel), and
293 most channel of active carbon was not dominated by the titanium dioxide [31]. The mesoporous
294 carbon with appropriate content may contribute to RhB molecules gather around TiO_2 particles in
295 low concentration solution of RhB, which improve the photocatalytic degradation process.
296 Therefore, the role of carbon pore structures is very important, which facilitate the diffusion of
297 RhB reactants and products on the TiO_2 active sites during the photocatalytic reaction. Similarly,
298 Pastravanu et al. [29] reported that even after 170 min of irradiation time, 92% MO was degraded
299 when the sample prepared through 7 min of microwave radiation was used as the photocatalyst;
300 nevertheless, only 42% of dye conversion was achieved in the case of pure TiO_2. The RhB removal
301 efficiencies followed the order of AC/TiO_2-700 W > AC/TiO_2-500 W > AC/TiO_2-300 W >
302 AC/TiO_2-900 W > AC/TiO_2-100 W. Nearly complete RhB photodegradation was further observed
303 when the microwave power was 700 W.

304 In a microwave oven, heat is generated from within the sample through the interaction of
305 microwaves with microwave-susceptible materials [25]. Therefore, the AC core was expected to
306 first interact with the microwaves to generate heat that will be transmitted to the TiO_2 shell,

resulting in the formation of the anatase phase (Fig. 1) at a relatively low power of 100 W. When the microwave power exceeded 100 W, the phase of rutile gradually formed. Many studies reported that the mixed-phase TiO_2 (anatase and rutile) exhibits higher photocatalytic activity than the pure phase because of the charge trapping and transfer at the phase interfaces of the mixed TiO_2 [5, 17, 23]. The anatase/rutile ratio is a more important factor in determining the photocatalytic activity of the prepared AC/TiO_2 through the formation of ·OH [21, 32]. With the increase of microwave power, the ratio of anatase/rutile decreased see in Table 1. When the power increased to 700 W, the ratio of anatase/rutile was 47/53, which was beneficial to the formation of ·OH. Lv et al. [22] reported the highest ·OH formation rate was observed when the two phase structures of anatase and rutile phases with a ratio of 57:43. Moreover, all the AC/TiO_2 composites exhibited higher PL intensity than pure TiO_2, suggesting that loading of TiO_2 on the surface of AC was a good route to induce the transfer and separation of the photogenerated charge carriers, which resulted in the increase of ·OH formation (Fig. 9). The following order was the generation rate of ·OH radicals of the catalysts: AC/TiO_2-700 W > AC/TiO_2-500 W > AC/TiO_2-300 W AC/TiO_2-900 W > AC/TiO_2-100 W > TiO_2. The result is in accordance with the photocatalytic activities of the photocatalysts in Fig. 8. So, the photocatalytic activity of the photocatalysts could be contributed to amounts of ·OH induced in the reaction system to some extent. The degradation mechanism for the AC/TiO_2 was similarly with the reported by Xiang et al. [23] that the activity of photocatalysts depending on the ·OH. In addition, surface area is another important factor in determining the photocatalytic activity of the prepared AC/TiO_2. The AC/TiO_2-100 W sample remained mostly amorphous TiO_2 which covered on the surface of AC because the maximum temperature reached was low with 30 min radiation. The amount of stable TiO_2 produced increased when the

microwave power was increased from 300 to 700 W, which resulted in an increase in TiO_2 loading on AC (Table 1). The rest of the amorphous TiO_2 detached from AC, thus increasing the exposed area of the carbon. Therefore, the photocatalytic effect of particles increased with increasing microwave power as evidenced by the synergistic relationship between AC and TiO_2. When the microwave power was increased to 900 W, the SBET significantly decreased because the high temperature induced TiO_2 agglomeration as shown in Fig. 3, resulting in decreased photolysis efficiency.

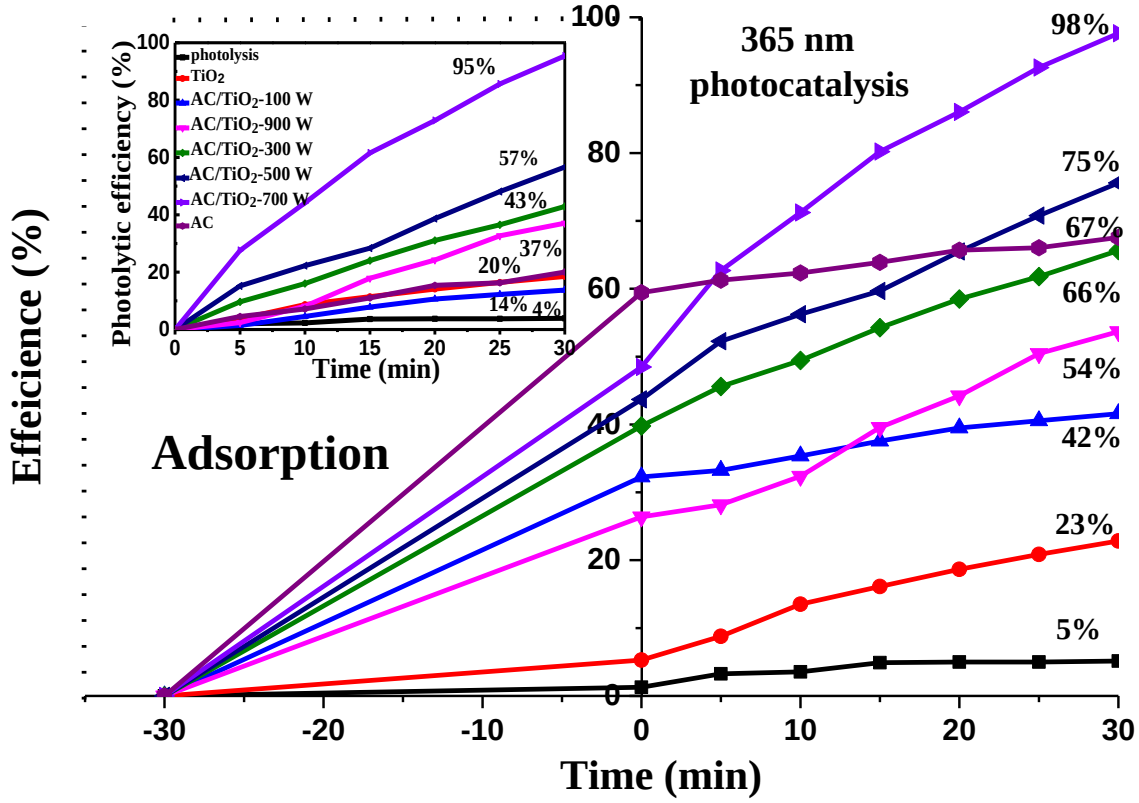

Fig. 8 RhB remove efficiencies over catalysts under 365 nm UV light (RhB concentration of 30 mg/L).

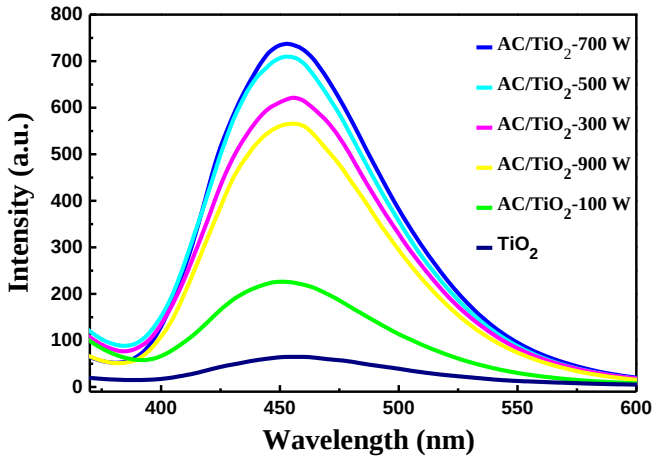

Fig. 9 PL spectra of pure TiO_2 and AC/TiO_2 prepared by different microwave conditions

3.9 Correlation analysis

The photocatalytic reaction process is complex and affected by several factors, such as TiO_2 content, morphology, and SBET. Correlation analysis was further conducted to study the effect of each factor on RhB removal efficiency. Fig. 10 shows that SBET and percentage composition of TiO_2 presented a good linear relationship to RhB removal efficiency in the tested AC/TiO_2 (R^2=0.6655 and R^2=0.8143). A high surface area of AC/TiO_2 with more TiO_2 content will generally result in high removal efficiency. Previous study showed that AC and TiO_2 has a synergetic effect on the photocatalytic RhB degradation, which could be ascribed to the enhanced adsorption of the pollutants on AC, followed by transfer from the interphase to titania, where the pollutants were photodegraded [19]. On the one hand, a large portion of the AC surface remained unoccupied, which shows that AC/TiO_2 still has very strong adsorptive capacity. Large SBET of the samples may dramatically enlarge the effective reaction surface areas between the photocatalysts and pollutants [5]. On the other hand, increased TiO_2 content could rapidly degrade RhB under irradiation. In addition, the correlation of microwave power (100-700 W) and removal efficiency has been shown in Fig.10 (c), which closed to the linear. So the AC/TiO_2-700 W sample was considered to own the highest photocatalytic activity, which was mainly attributed to the high

sorption properties of mesoporous carbon material and high amount of TiO_2. Thus, the surface area and TiO_2 content of AC/TiO_2 should be as high as possible to improve AC/TiO_2 performance for RhB photocatalytic degradation.

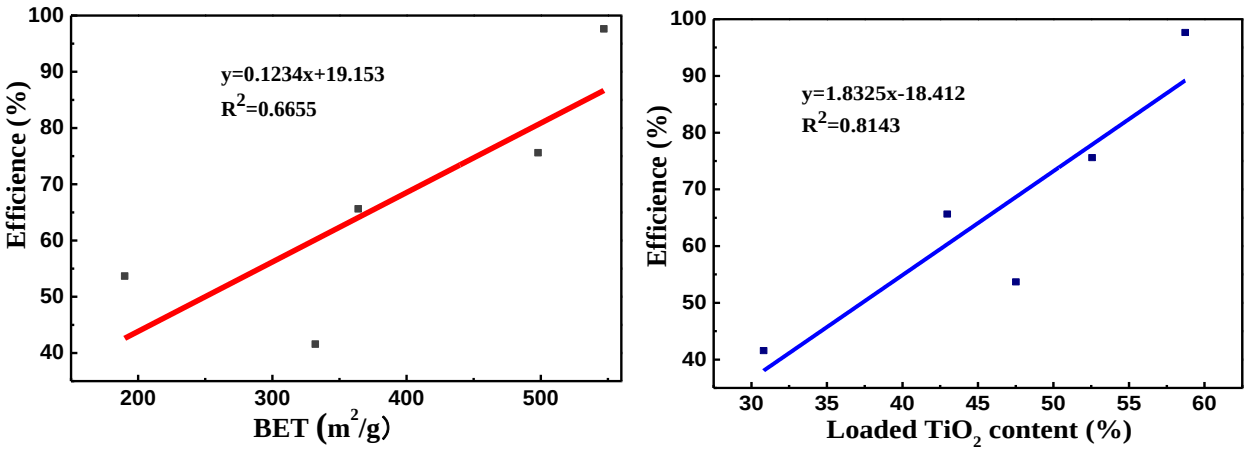

(a) (b)

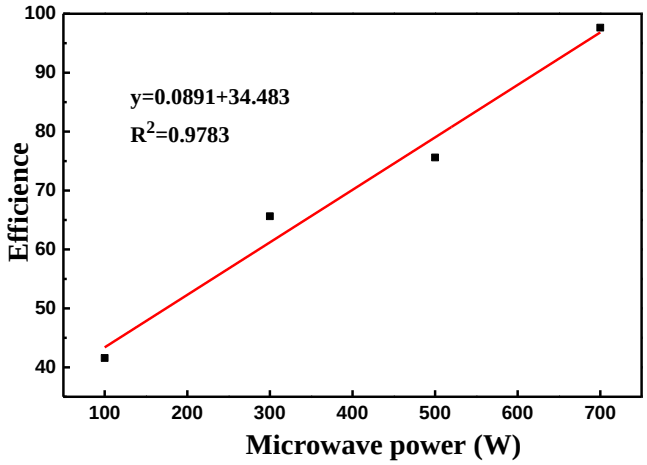

(c)

Fig.10. (a) BET surface area and remove efficiency of RhB (b) loaded TiO_2 content and remove efficiency of RhB (c) microwave power (100-700 W) and remove efficiency of RhB

4. Conclusions

In this study, AC/TiO_2 nanocomposites were efficiently prepared using microwave radiation technology. The proposed method features simplicity, flexibility, short reaction times, and high photocatalytic efficiency. XRD analysis confirmed that TiO_2 nanoparticles are anatase and rutile

with a particle size of 20–50 nm. The SEM and TEM analyses indicated that TiO_2 nanoparticles are spherical in shape and well distributed on the AC surface. The SBETs of the AC/TiO_2 composites decreased with increasing TiO_2 loading, but a large portion of the AC surface remained unoccupied. From the UV-vis spectrum, an obvious red-shift was observed when TiO_2 coated the AC surface. The efficiency of the samples followed the order: AC/TiO_2-700 W > AC/TiO_2-500 W > AC/TiO_2-300 W > AC/TiO_2-900 W > AC/TiO_2-100 W > TiO_2, which was related to the formation rate of ·OH. For AC/TiO_2-700 W, the removal efficiency of RhB reached to 98% after 30 min of UV irradiation. The high surface area with high TiO_2 content of AC/TiO_2 showed good RhB photocatalytic degradation. The proposed method for preparation of photocatalysts with improved structural features and excellent photocatalytic effect can be easily implemented and is economical, and the resulting composite can be potentially applied in water pollution treatment.

Acknowledgements

This work was supported financially by funding from the National Natural Science Foundation of China (51262025), International scientific and technological cooperation project of Xinjiang Bingtuan (2013BC002) and Graduate Research Innovation Project in Xinjiang (XJGRI2014053).

References

[1] N. Guo, Y.M. Liang, S. Lan, L. Liu, G.J. Ji, S.C. Gan, H.F. Zou, X.C. Xu, Uniform TiO_2-SiO_2 hollow nanospheres: synthesis, characterization and enhanced adsorption–photodegradation of azo dyes and phenol, Appl. Surf. Sci. 305 (2014) 562-574.

[2] S.F. Chen,Y.F. Hu, S.G. Meng, X.L. Fu, Study on the separation mechanisms of photogenerated electrons and holes for composite photocatalysts g-C_3N_4-WO_3, Appl. Catal. B-Environ. 150-151 (2014) 564-573.

[3] N. Todorova, T. Giannakopoulou, S. Karapati, D. Petridis, T. Vaimakis, C. Trapalis, Composite TiO_2/clays materials for photocatalytic NO_x oxidation, Appl. Surf. Sci. 319 (2014) 113-120.
[4] L. Gomathi Devi, S. Girish Kumar, B. Narasimha Murthy, Nagaraju Kottam, Influence of Mn^{2+} and Mo^{6+} dopants on the phase transformations of TiO_2 lattice and its photo catalytic activity under solar illumination., Catal. Commun. 10 (2009) 794-798.
[5] S. Photong, V. Boonamnuayvitaya, Preparation and characterization of amine-functionalized SiO_2/TiO_2 films for formaldehyde degradation, Appl. Surf. Sci. 255 (2009) 9311-9315.
[6] W.J. Liang, J. Li, Y.Q. Jin, Photo-catalytic degradation of gaseous formaldehyde by TiO_2/UV, Ag/TiO_2/UV and Ce/TiO_2/UV, Build. Environ. 51 (2012) 345-350.
[7] Z. Ma, Cobalt oxide catalysts for environmental remediation, Current Catalysis 3 (2014) 15-26.
[8] D.G. Calatayud, T. Jardiel, M. Peiteado, A.C. Caballero, D. Fernández-Hevia, Microwave-induced fast crystallization of amorphous hierarchical anatase microspheres, Nanoscale Res. Lett. 9 (2014) 273-278.
[9] S. Girish Kumar, K.S.R. Koteswara Rao, Zinc oxide based photocatalysis: tailoring surface-bulk structure and related interfacial charge carrier dynamics for better environmental applications, RSC Adv. 5 (2015) 3306-3351.
[10] L. Gomathi Devi, R. Kavitha, Review on modified N-TiO_2 for green energy applications under UV/visible light: selected results and reaction mechanisms, RSC Adv. 4 (2014) 28265-28299.
[11] L.F. Chiang, R. Doong, Cu-TiO_2 nanorods with enhanced ultraviolet- and visible-lightphotoactivity for bisphenol A degradation, J. Hazard. Mater. 277 (2014) 84-92.
[12] S.G. Liu, J.G. Yu, B. Cheng, M. Jaroniec, Fluorinated semiconductor photocatalysts: Tunable synthesis and unique properties, Adv. Colloid Interfac. 173 (2012) 35-53.
[13] L. Gomathi Devi, R. Kavitha, A review on non metal ion doped titania for the photocatalytic degradation of organic pollutants under UV/solar light: Role of photogenerated charge carrier dynamics in enhancing the activity, Appl. Catal. B-Environ. 140-141 (2013) 559-587.
[14]S. Girish Kumar, L. Gomathi Devi , Review on modified TiO_2 photocatalysis under UV/visible light: selected results and related mechanisms on interfacial charge carrier transfer dynamics, J. Phys. Chem. A 115 (2011) 13211-13241.
[15] Z. Zhang, Y. Xu, X. Ma, F. Li, D. Liu, Z. Chen, F. Zhang, D.D. Dionysiou, Microwave degradation of methyl orange dye in aqueous solution in the presence of nano-TiO_2-supported activated carbon (supported-TiO_2/AC/MW). J. Hazard. Mater. 209-210 (2012) 271-277.
[16] J.G. Yu, M. Jaroniec, Photocatalytic materials for energy and environmental applications, Appl. Surf. Sci. 319 (2014) 136-142.
[17] F. Teng, G.Z. Zhang, Y.Q. Wang, C.T. Gao, L.L. Chen, P. Zhang, Z.X. Zhang, E.Q. Xie, The role of carbon in the photocatalytic reaction of carbon/TiO_2 photocatalysts, Appl. Surf. Sci. 320 (2014) 703-709.
[18] G.H. Li, K.A. Gray, The solid-solid interface: Explaining the high and unique photocatalytic reactivity of TiO_2-based nanocomposite materials, Chem. Phys. 339 (2007) 173-187.
[19] S. Girish Kumar, K.S.R. Koteswara Rao, Polymorphic phase transition among the titania crystal structures using a solution-based approach: from precursor chemistry to nucleation process, Nanoscale 6 (2014) 11574-11632.
[20] M.L. Chen, J.S. Bae, W.Ch. Oh, Characterization of AC/TiO_2 composite prepared with pitch binder and their photocatalytic activity, B. Kor. Chem. Soc. 27 (2006) 1423-1228.

[21] H. Xu, L.Z. Zhang, Controllable one-pot synthesis and enhanced photocatalytic activity of mixed-phase TiO_2 nanocrystals with tunable brookite/rutile ratios, J. Phys. Chem. C, 113 (2009) 1785-1790.
[22] K. Lv, J.G. Yu, K.J. Deng, X.H. Li, M. Li, Effect of phase structures on the formation rate of hydroxyl radicals on the surface of TiO_2. J. Phys. Chem. Solids 71 (2010) 519-522.
[23] Q.J. Xiang, J.G. Yu, Quantitative characterization of hydroxyl radicals produced by various photocatalysts, J. Colloid Interf. Sci. 357 (2011) 163-167.
[24] X.M. Xiao, F. Tian, Y.J. Yan, Z.S. Wu, Adsorption behavior of pyrene from onto coal-based activated carbons prepared by microwave activation, J. Shihezi Univ. 32 (2014) 485-490.
[25] Y. Wang, J.G. Yu, W. Xiao, Q. Li, Microwave-assisted hydrothermal synthesis of graphene based Au-TiO_2 photocatalysts for efficient visible-light hydrogen production, J. Mater. Chem. A 2 (2014) 3847-3855.
[26] P. Chen, J.D. Peng, C.H. Liao, P.S. Shen, P.L. Kuo, Microwave-assisted hydrothermal synthesis of TiO_2 spheres with efficient photovoltaic performance for dye-sensitized solar cells, J. Nanopart. Res. 15 (2013) 1465-1476.
[27] K.-i. Ishibashi, A. Fujishima, T. Watanabe, K. Hashimoto, Detection of active oxidative species in TiO_2 photocatalysis using the fluorescence technique, Electrochem. Commun. 2 (2000) 207-210.
[28] J.C. Sin, S.M. Lam, I. Satoshi, K.T. Lee, A.R. Mohamed, Sunlight photocatalytic activity enhancement and mechanism of novel europium-doped ZnO hierarchical micro/nanospheres for degradation of phenol. Appl. Catal. B-Environ. 148-149 (2014) 258-268.
[29] C. Coromelci-Pastravanu, M. Ignat, E. Popovici, V. Harabagiu, TiO_2-coated mesoporous carbon: Conventional vs. microwave-annealing process, J. Hazard. Mater. 278 (2014) 382-390.
[30] X.M. Xiao, D.D. Liu, Y.J. Yan, Z. Wu, Z.S. Wu, G. Cravotto, Preparation of activated carbon from Xinjiang region coal by microwave activation and its application in naphthalene, phenanthrene, and pyrene adsorption, J. Taiwan Inst. Chem. E. 000 (2015) 1-8.
[31] F Tian, Z.S. Wu, Y.J. Yan, X.Y Ge, Y.B. Tong, Photodegradation of formaldehyde by activated carbon loading TiO_2 synthesized via microwave irradiation, Korean J. Chem. Eng. 2015, DOI:10.1007/s11814-014-0338-2.
[32] L. Gomathi Devi, N. Kottam, S. Girish Kumar, Preparation and characterization of Mn-doped titanates with a bicrystalline framework: Correlation of the crystallite size with the synergistic effect on the photocatalytic activity, J. Phys. Chem. C 113 (2009) 15593-15601.